Angular momentum effects in fission

R. Vogt [1,2,*] and J. Randrup [3]

[1]*Nuclear and Chemical Sciences Division, Lawrence Livermore National Laboratory, Livermore, California 94551, USA*

[2]*Physics and Astronomy Department, University of California, Davis, Davis, California 95616, USA*

[3]*Nuclear Science Division, Lawrence Berkeley National Laboratory, Berkeley, California 94720, USA*

(Received 13 October 2020; accepted 22 December 2020; published 19 January 2021)

Background: The role of angular momentum in fission has long been discussed but the observable effects are difficult to quantify.

Purpose: We discuss a variety of effects associated with angular momentum in fission and present quantitative illustrations.

Methods: We employ the fission simulation model FREYA, which is well suited for this purpose because it obeys all conservation laws, including linear and angular momentum conservation at each step of the process. We first discuss the implementation of angular momentum in FREYA and then assess particular observables, including various correlated observables. We also study potential effects of neutron-induced fission of the low-lying isomeric state of ^{235}U relative to the ground state.

Results: The fluctuations inherent in the fission process ensure that the spin of the initial compound nucleus has only a small influence on the fragment spins, which are therefore nearly uncorrelated. There is a marked correlation between the spin magnitude of the fission fragments and the photon multiplicity. We also consider the dynamical anisotropy caused by the rotation of an evaporating fragment and study especially the distribution of the projected neutron-neutron opening angles, showing that while it is dominated by the effect of the evaporation recoils, it is possible to extract the signal of the dynamical anisotropy by means of a Fourier decomposition. Finally, we note that the use of an isomeric target, ^{235m}U($n_{\rm th}$,f), may enhance the symmetric yields and can thus result in higher neutron multiplicities for low total fragment kinetic energies.

Conclusions: While the initial angular momentum of the fissioning nucleus tends to have little effect on the observables, those of the produced fragments influence the emitted neutrons and photons in a significant and correlated manner which may be exploited experimentally to elucidate the fission process.

DOI: 10.1103/PhysRevC.103.014610

I. INTRODUCTION

The role of angular momentum in nuclear fission has long been a topic of central interest, dating back over 60 years. Experimental evidence suggests that the primary fission fragments on average carry spins of magnitude $5\hbar-7\hbar$ aligned roughly perpendicular to the fission axis [1]. The associated fragment rotation generally causes the neutron evaporation to be anisotropic [2,3], which may affect a variety of neutron-related observables, including neutron spectra, angular distributions, and directional correlations [4], as well as attempts to find evidence of scission neutrons [2,5,6]. The fragment angular momentum also influences the photon radiation [7].

For the purpose of elucidating the various ways angular momentum enters into the fission process and to quantitatively ascertain the effect on observables of particular interest, the present study utilizes the event-by-event fission model FREYA [8,9], which uses Monte Carlo techniques to generate large samples of complete fission events. An important advantage of employing FREYA is that all conservation laws are obeyed throughout each fission event, including those affecting the angular momentum directions during the evaporation cascades.

Section II describes how angular momentum is treated in FREYA. Section III addresses observables of particular interest. Then Sec. IV describes potential observable differences in ^{235}U($n_{\rm th}$,f) arising if the target nucleus is in its isomeric state. Our concluding remarks are presented in Sec. V.

II. TREATMENT OF ANGULAR MOMENTUM IN FREYA

FREYA is a Monte Carlo model that is capable of quickly generating large samples of complete fission events, namely, the full kinematic information for the two prompt product nuclei and all prompt neutrons and photons in each event. With these large samples, it is straightforward to extract any observable of interest. Because each fission event conserves mass, charge, energy, linear and angular momentum, and spin, any inherent correlations between various quantities are preserved, thus making FREYA particularly well suited for determining how angular momentum affects various final states.

Angular momentum enters at several stages during the fission process. In the following section, we describe how it is treated in FREYA.

*rlvogt@lbl.gov

A. Preparation

During the first stage of a neutron-induced fission event, a neutron of momentum $\boldsymbol{p}_0$ impinges on the target nucleus, in the present case ^{235}U. The associated impact parameter ρ is chosen randomly from a disk, perpendicular to the direction of motion, with a radius equal to that of the nucleus. Thus the neutron introduces a linear momentum of $\boldsymbol{p}_0$ and an angular momentum of $\boldsymbol{\rho} \times \boldsymbol{p}_0$.

The incoming neutron may cause the emission of a preequilibrium neutron. While preequilibrium processes grow increasingly likely at higher energies, they are unimportant at thermal energies. If preequilibrium emission does occur, the appropriate reduction is made of the mass number as well as the linear and angular momenta of the residual system, which is assumed to subsequently relax to a compound nucleus which can ultimately fission.

If sufficiently excited, the compound nucleus may evaporate one or more neutrons before fission occurs, according to the energy-dependent branching ratio $\Gamma_n/\Gamma_\mathrm{f}$. Such prefission evaporation is treated the same way as the postfission evaporation from the fission fragments (see Sec. II C). For each evaporation, FREYA reduces the excitation energy of the daughter nucleus and changes its linear and angular momenta as dictated by conservation laws.

At the end of the prefission evaporation chain, we arrive at the fissioning nucleus with angular momentum $\boldsymbol{S}_0$, which has generally been reoriented relative to $\boldsymbol{\rho} \times \boldsymbol{p}_0$ due to the spin recoils, by about 24° on average for ^{235}U(n,f) for an incoming neutron energy of $E_n = 20$ MeV.

B. Scission

The second stage of the fission process is the evolution of the prefission compound nucleus to two well-separated and fully accelerated primary fragments, each of which is also in equilibrium. It is not the purpose of FREYA to model how this complicated time-dependent many-body process develops. (That challenging problem was recently reviewed in Ref. [10] and a broader review of the recent experimental and theoretical progress in fission can be found in Ref. [11].) Rather, FREYA generates an ensemble of possible outcomes based primarily on the input provided. Generally, the FREYA input is based on experimental data, but a certain degree of modeling is necessary because the data sets are often incomplete. For example, while experimental data for the fragment mass distribution $Y(A)$ and the associated mean total fragment kinetic energy $\overline{\mathrm{TKE}}(A)$ are often available for thermal neutron-induced fission, the energy dependence of these functions is usually not well measured.

After the neutron and proton numbers of the primary fragments have been selected, their angular momenta are sampled from the statistical distribution of the dinuclear rotational modes at scission [12]. The total angular momentum of the system after scission is given by $\boldsymbol{S}_0 = \boldsymbol{S}_L + \boldsymbol{S}_H + \boldsymbol{L}$, namely, the sum of the two individual light- and heavy-fragment spins and the orbital angular momentum of the two-fragment system, $\boldsymbol{L} = \boldsymbol{R} \times \boldsymbol{P}$, where $\boldsymbol{R} = \boldsymbol{R}_L - \boldsymbol{R}_H$ is the fragment separation and $\boldsymbol{P} = \mu(\boldsymbol{V}_L - \boldsymbol{V}_H)$ is the associated momentum, equal to the reduced mass $\mu = M_L M_H/(M_L + M_H)$ times their relative velocity. The overall rotation of the dinuclear complex determines the average values of the fragment spins, $\overline{\boldsymbol{S}}_i = (\mathcal{I}_i/\mathcal{I})\boldsymbol{S}_0$, as well as the average of their relative angular momentum, $\overline{\boldsymbol{L}} = (\mathcal{I}_R/\mathcal{I})\boldsymbol{S}_0$. Here $\mathcal{I}_i$ is the moment of inertia of fragment $i = L, H$, $\mathcal{I}_R = \mu R^2$ is the moment of inertia for the relative motion, and $\mathcal{I} = \mathcal{I}_L + \mathcal{I}_H + \mathcal{I}_R$ is the total moment of inertia. (The nuclear moments of inertia are taken to be 50% of the rigid-body values, as is commonly done.)

Because the system is excited at the time of scission, the intrinsic rotational modes are expected to be agitated and the actual angular momenta will therefore fluctuate, $\boldsymbol{S}_i = \overline{\boldsymbol{S}}_i + \delta\boldsymbol{S}_i$. In order to sample the spin fluctuations, $\delta\boldsymbol{S}_i$, FREYA brings the rotational energy,

$$E^{\mathrm{rot}} = S_L^2/2\mathcal{I}_L + S_H^2/2\mathcal{I}_H + L^2/2\mathcal{I}_R, \tag{1}$$

into normal form [9,12]. A binary system generally has six normal modes of rotation [13]. These are *tilting* and *twisting*, in which the fragments rotate in the same or in the opposite sense around the dinuclear axis $\hat{\boldsymbol{z}} = \boldsymbol{R}/R$, and *wriggling* and *bending*, in which they rotate in the same or in the opposite sense around an axis perpendicular to the dinuclear axis [14,15]. The latter two modes are each doubly degenerate (corresponding to rotations around $\hat{\boldsymbol{x}}$ and $\hat{\boldsymbol{y}}$, for example.) Only the perpendicular modes (wriggling and bending) are considered by FREYA [9,12], because the agitation of the first two tends to be suppressed due to the constricted neck [13].

The rotational energy associated with the four perpendicular modes can be written in normal form as

$$E_\perp^{\mathrm{rot}} = s_+^2/2\mathcal{I}_+ + s_-^2/2\mathcal{I}_-, \tag{2}$$

where $\boldsymbol{s}_+$ represents wriggling and $\boldsymbol{s}_-$ represents bending. The corresponding moments of inertia are [13]

$$\mathcal{I}_+ = (\mathcal{I}_L + \mathcal{I}_H)\mathcal{I}/\mathcal{I}_R, \quad \mathcal{I}_- = \mathcal{I}_L\mathcal{I}_H/(\mathcal{I}_L + \mathcal{I}_H). \tag{3}$$

FREYA then samples $\boldsymbol{s}_\pm$ from a distribution of statistical form, $P(\boldsymbol{s}_\pm) \sim \exp(-s_\pm^2/2\mathcal{I}_\pm T_S)$, where T_S is the effective spin temperature (explained below).

The resulting angular momenta of the individual fragments are subsequently obtained as

$$\boldsymbol{S}_L = \overline{\boldsymbol{S}}_L + \delta\boldsymbol{S}_L = (\mathcal{I}_L/\mathcal{I})\boldsymbol{S}_0 + (\mathcal{I}_L/\mathcal{I}_+)\boldsymbol{s}_+ + \boldsymbol{s}_-, \tag{4}$$

$$\boldsymbol{S}_H = \overline{\boldsymbol{S}}_H + \delta\boldsymbol{S}_H = (\mathcal{I}_H/\mathcal{I})\boldsymbol{S}_0 + (\mathcal{I}_H/\mathcal{I}_+)\boldsymbol{s}_+ - \boldsymbol{s}_-. \tag{5}$$

The fluctuations $\boldsymbol{s}_+$ and $\boldsymbol{s}_-$ are oriented randomly in the plane perpendicular to the dinuclear axis. The wriggling mode adds parallel fluctuations to the fragment spins, while the contributions from the bending mode are antiparallel. There is thus no simple relationship between the direction of the two resulting fragment spins, $\boldsymbol{S}_L$ and $\boldsymbol{S}_H$, as we now discuss in more detail.

As brought out in Eqs. (4) and (5), there are two distinct contributions to the angular momentum of a primary fragment, namely, the fragment's share of the overall rotation of the dinuclear complex, $\overline{\boldsymbol{S}}_i$, and the fluctuations received at scission, $\delta\boldsymbol{S}_i$. It is important to recognize that the latter generally dominate.

To understand this important feature, we first note that the angular momentum brought in by a thermal neutron is negligible, $S_0 \approx 0.34\hbar$ on average. At an incoming energy

of $E_n = 20$ MeV the angular momentum of the fissioning compound nucleus is $S_0 \approx 5\hbar$. However, at scission where the total angular momentum is divided between the two fledgling fragments and their relative motion, the former acquire only small fractions because their moments of inertia are relatively small, $\mathcal{I}_i \ll \mathcal{I}_R$. Consequently, even for $E_n = 20$ MeV, this contribution amounts to only $\approx 0.26\hbar$ on average for ^{235}U(n,f) (this would increase to $\approx 0.48\hbar$ if the full rigid values were used for the fragment moments of inertia).

The magnitude of the spin fluctuations is governed by the degree of internal excitation at scission, $E^*_{\rm sc}$. Because this quantity depends on how much of the total excitation energy (TXE) is tied up in distortion energy, it is not readily available and FREYA therefore employs an effective value given by $c_S^2 \cdot \mathrm{TXE} = a_0 T_S^2$, where the reduction factor c_S is a parameter in FREYA and the level-density parameter a_0 is calculated assuming a back-shifted Fermi gas [16]. (For ^{235}U(n,f) FREYA uses $c_S = 0.87$; one can elucidate the effects of the spin fluctuations by varying c_S; see Ref. [7].) Starting from $\approx$22 MeV for thermal fission, the TXE increases steadily to $\approx$40 MeV at $E_n = 20$ MeV, so the effective spin temperature T_S is in the range 0.85–1.15 MeV. The mean spin fluctuations $[\langle(\delta S_i)^2\rangle]^{1/2}$ are then $4.8\hbar/6.4\hbar$, for the light/heavy fragment in thermal fission and $5.8\hbar/7.1\hbar$ for $E_n = 20$ MeV (or about 2 units more if the rigid body moments of inertia are used). Thus, generally, the spin fluctuation is over an order of magnitude larger than the aligned component. Consequently, the fragment spins are primarily determined by the fluctuations acquired at scission.

As discussed above, the fragments themselves inherit only a small fraction of the total angular momentum in the system, with the main part going to the relative motion. Because the spin fluctuations dominate over the averages, there is very little correlation remaining between the directions of the resulting total fragment spins $\boldsymbol{S}_i$ and the direction of the overall angular momentum $\boldsymbol{S}_0$, aside from them all being perpendicular to the dinuclear axis. (Note that the relative orbital angular momentum $\boldsymbol{L}$ is adjusted to counteract the bending-mode fluctuations, ensuring conservation of the total angular momentum.)

Furthermore, the two individual fragment spins are also rather uncorrelated. Indeed, ignoring the small aligned component $\overline{\boldsymbol{S}}_i$ [see Eqs. (4) and (5)], i.e., assuming $\boldsymbol{S}_i \approx \delta\boldsymbol{S}_i$, we find

$$\begin{aligned}\langle S_i^2\rangle &\approx \left(\mathcal{I}_i^2/\mathcal{I}_+^2\right)\langle s_+^2\rangle + \langle s_-^2\rangle = 2\left(\left(\mathcal{I}_i^2/\mathcal{I}_+\right) + \mathcal{I}_-\right)T_S \\ &= 2\mathcal{I}_i(1 - \mathcal{I}_i/\mathcal{I})T_S \approx 2\mathcal{I}_i T_S. \end{aligned} \tag{6}$$

Thus the resulting fragment spins are approximately equivalent to statistical sampling without preserving any conservation laws. The ratio between the wriggling and the bending terms in Eq. (6) is $\approx \mathcal{I}_H/\mathcal{I}_L$ for $\langle S_L^2\rangle$, while it is $\approx \mathcal{I}_L/\mathcal{I}_H$ for $\langle S_H^2\rangle$. Thus the two types of modes contribute about equally to the fragment spins. It then follows that their directional correlation is rather weak.

This overall weak directional correlation can be quantitatively observed in Fig. 1, which shows $P(\phi_{\rm LH})$, the distribution of the opening angle between the two spins. For a given mass partition, this distribution does not depend on the incident

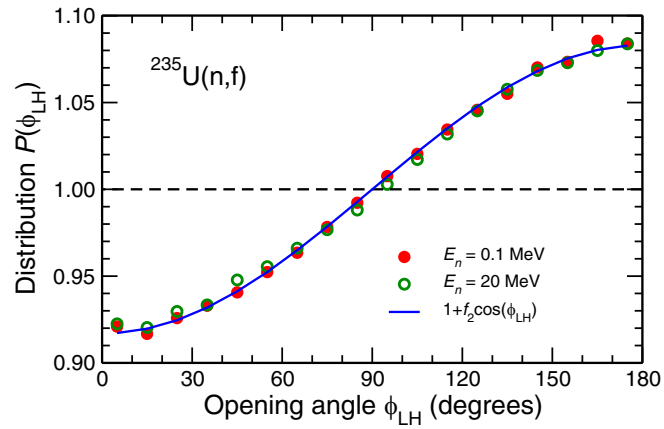

FIG. 1. The distribution of the opening angle $\phi_{\rm LH}$ between the spins of the two primary fission fragments from ^{235}U(n,f) for two neutron energies: thermal neutrons and $E_n = 20$ MeV. Also shown is the lowest-order Fourier approximation, $P(\phi_{\rm LH}) = 1 + f_2 \cos\phi_{\rm LH}$.

energy because the spin fluctuations scale with T_S. Furthermore, because the moments of inertia of the fragments are so small compared to the relative moment of inertia there is also very little dependence on the mass partition. Thus $P(\phi_{\rm LH})$ is a fairly universal function. We note that it can be represented to a very good approximation as $P(\phi_{\rm LH}) \approx 1 + f_2 \cos\phi_{\rm LH}$, with Fourier amplitude $f_2 \approx -0.082$. Thus the two fragment spins have a slight preference for being oppositely directed, with $P(180^\circ)/P(0^\circ) \approx 1.18$.

It should be noted that because the wriggling mode contributes parallel spin fluctuations, conservation of angular momentum causes the orbital angular momentum L to be affected oppositely, $\delta\boldsymbol{L} = -(\mathcal{I}_R/\mathcal{I})\boldsymbol{s}_+$. This changes not only the magnitude of L but also its orientation. Therefore the plane of the relative fragment motion (the exit plane) generally differs from the impact plane. FREYA takes this into account when calculating the orbital Coulomb trajectory of the receding fragments. Furthermore, because the Coulomb trajectory is hyperbolic, the asymptotic direction of the relative fragment motion differs from the orientation of the system at scission. However, as a result of the relative slowness of the orbital fragment motion at scission and the strong radial acceleration from the mutual Coulomb repulsion, the associated reorientation angle is rather small, amounting typically to about 2°.

C. Fragment deexcitation

After their formation and acceleration, the excited primary fragments undergo a sequence of decay processes. FREYA first considers neutron evaporation, starting by calculating the available statistical excitation energy for each fragment, $Q_i = E_i^* - E_i^{\rm rot}$, where E_i^* is its total excitation energy and its rotational energy is given by $E_i^{\rm rot} = S_i^2/2\mathcal{I}_i$. If the statistical energy exceeds the neutron separation energy, S_n, then evaporation can occur. The neutron is evaporated with a black-body spectrum from a randomly selected point on the surface of the rotating fragment. The local rotational velocity of the surface element adds a centrifugal boost to the neutron. The daughter fragment absorbs the resulting linear and angular momentum

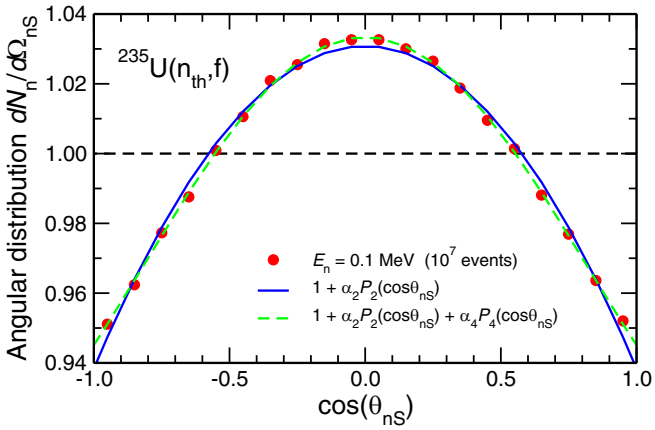

FIG. 2. The angular distribution of the evaporated neutrons relative to the spin direction of the emitting fragment, $dN_n/d\Omega_{nS}$, averaged over the evaporation chains for the entire fragment yield distribution from ^{235}U($n_{\rm th}$,f). In addition to the FREYA simulation results (filled red circles), the lowest two Legendre approximations are shown.

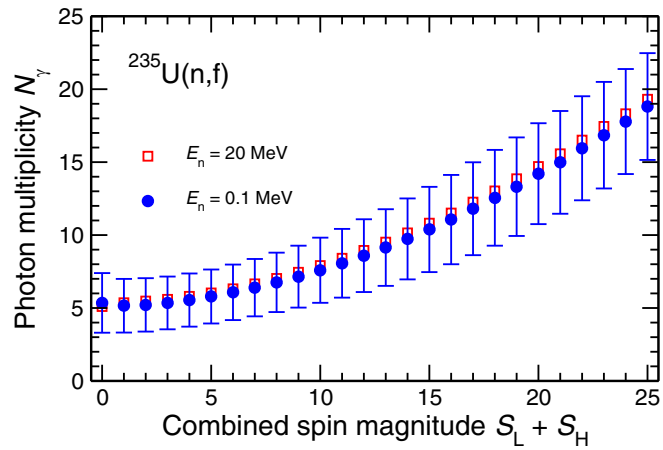

FIG. 3. The mean number of photons emitted from ^{235}U($n_{\rm th}$,f) (filled blue circles) as a function of the sum of the two primary fragment spin magnitudes, $S = S_L + S_H$. The associated event-by-event photon multiplicity dispersion is indicated by the vertical bars. Also shown are the mean multiplicities for $E_n = 20$ MeV (open red squares).

recoils. This procedure is iterated as long as evaporation is energetically allowed.

The centrifugal boost from the fragment rotation causes the angular distribution of the evaporated neutrons to be anisotropic, with an enhancement in the equatorial plane, as illustrated in Fig. 2. The degree of bulging may be expressed in terms of the so-called dynamical anisotropy [6],

$$A \equiv \left[\frac{dN_n}{d\Omega_{nS}}\right]_{\theta_{nS}=90^\circ} \Bigg/ \left[\frac{dN_n}{d\Omega_{nS}}\right]_{\theta_{nS}=0^\circ} - 1, \qquad (7)$$

which is ≈ 0.093 for ^{235}U($n_{\rm th}$,f). The fragment evaporation chains lead to a reorientation of the fragment spins by $\approx 13^\circ$ on average, while the spin magnitudes are reduced only very slightly, by $\approx 0.06\,\hbar$ on average.

After evaporation has ceased, the resulting product nucleus disposes of its remaining excitation energy and angular momentum by photon emission. First, the statistical excitation energy is radiated away by emission of E1 and M1 photons, each one changing the nuclear spin by 1 unit. The statistical radiation brings the system to the yrast line, where $E_i^* = E_i^{\rm rot}$. The nucleus then starts emitting stretched quadrupole photons. At some point, the excitation reaches the regime tabulated in the RIPL database [17] and FREYA then simulates those transitions until the ground state, or a sufficiently long-lived isomeric state, is reached. (The further fate of a prompt product nucleus due to β processes is not yet considered in FREYA.)

For the present study, it is interesting to note that there is a relatively tight correlation between the initial fragment spin magnitude and the number of photons emitted, as brought out in Fig. 3. This relationship is fairly universal: it is approximately independent of the incident neutron energy and it changes by only a fraction of a unit between ^{233}U(n,f) and Cf(sf). When the combined spin magnitudes, $S \equiv S_{\rm L} + S_{\rm H}$, exceeds $\approx 6\hbar$, there is a clear increase in $\overline{N}_\gamma$ with S, with roughly one additional photon emitted for each additional unit of total fragment angular momentum. As may be expected, the relationship is sensitive to the degree of reduction of the fragment moment of inertia, $c_I \equiv \mathcal{I}/\mathcal{I}_{\rm rigid}$. For $c_I = 0.5$, the value used throughout the present study, the slope for large S is $d\overline{N}_\gamma/dS \approx 0.84$, while it is ≈ 1.06 for $c_I = 0.3$. Because of this feature, the measurement of the photon multiplicity may, to some degree, substitute for the measurement of the total fragment angular momenta (see Fig. 6).

III. RESULTS

In this section, results are presented for observables that may elucidate behavior caused by the fragment angular momenta. We begin with observables related to the neutron distribution relative to the direction of the primary fragment. We then discuss neutron-neutron correlations gated on the fragment angular momentum, using photon multiplicity as a proxy. Finally, we examine a recently proposed observable [6] based on the transverse neutron motion.

As mentioned in the previous section, the neutrons evaporated from rotating fission fragments have a slight preference for emission perpendicular to the angular momentum due to the centrifugal boost. Simulations with FREYA show that the angular distribution,

$$\frac{dN_n}{d\Omega_{nS}} \sim 1 + \alpha_2 P_2(\cos\theta_{nS}) + \alpha_4 P_4(\cos\theta_{nS}) + \cdots, \qquad (8)$$

where the polar angle θ_{nS}, defined with respect to the direction of the mother fragment spin, is well described by the second-order Legendre approximation (see Fig. 2). When averaging over all events (i.e., over the impact parameter, mass, charge, and TKE, as well as the associated evaporation cascades), FREYA gives $\alpha_2 = -0.061$ and $\alpha_4 = 0.0056$ for ^{235}U($n_{\rm th}$,f).

Because the orientation χ of the fragment spin in the plane perpendicular to the fragment motion is unknown, averaging over χ turns the inherently oblate emission pattern in Eq. (8)

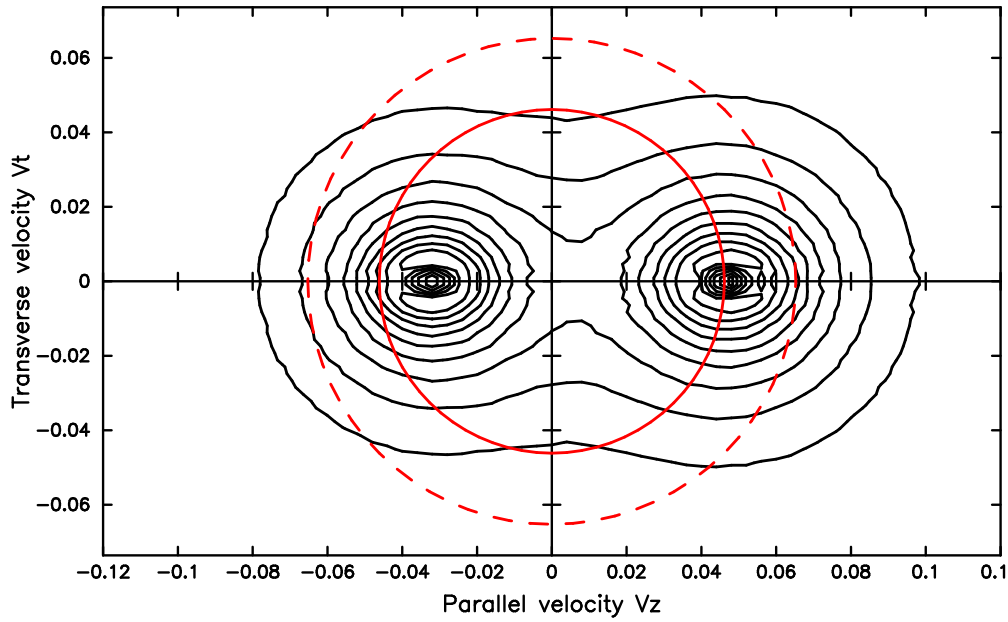

FIG. 4. A contour plot of the velocity distribution of neutrons evaporated following ^{235}U($n_{\rm th}$,f) is shown. The z direction is chosen to be along the motion of the light primary fragment in each event. Red circles have radii corresponding to constant neutron kinetic energies of 1 MeV (solid) and 2 MeV (dashed).

into a prolate shape with its symmetry axis along the fragment direction. In the frame of the moving fragment, the distribution of θ_{nF}, the angle between the neutron velocity and that of the fragment, is

$$\left\langle \frac{dN_n}{d\Omega_{nF}} \right\rangle_\chi \sim 1 - \alpha_2' P_2(\cos\theta_{nF}) + \alpha_4' P_4(\cos\theta_{nF}) + \ldots . \quad (9)$$

It can generally be shown that the coefficients in Eq. (9) are related to those in Eq. (8) by $\alpha_{2n}' = (-1)^n \langle \cos^{2n}\chi \rangle \alpha_{2n}$, where $\langle \cos^{2n}\chi \rangle = (2n!)/[2^{2n}(n!)^2]$ is the average over the spin direction χ. We thus have $\alpha_2' = -\frac{1}{2}\alpha_2$, $\alpha_4' = \frac{3}{8}\alpha_4$, $\alpha_6' = -\frac{5}{16}\alpha_6$, and so on.

A. Angular distribution

The distributions in Eqs. (8) and (9) are not directly observable and must be transformed to the laboratory frame, with the associated boost velocity depending on the mass and kinetic energy of each fragment. Figure 4 shows a contour plot of the resulting combined velocity distribution of the neutrons from both fragments in each event, $dN_n/d^3\boldsymbol{v}$, for ^{235}U($n_{\rm th}$,f). Even though the distribution retains the axial symmetry of the contributions from each fragment, it is forward-backward asymmetric because the light fragment moves faster and tends to evaporate more neutrons. The circles centered at the origin represent constant neutron kinetic energies of 1 and 2 MeV. They make it apparent that introducing an energy threshold will enhance the forward-backward character of the emission pattern.

The resulting angular distribution with respect to the direction of the light fragment, $P(\cos\theta_{nL})$, follows from the dumbbell-shaped distribution shown in Fig. 4. The boost enhances the yield in the forward direction, $\cos\theta_{nL} > 0$, and depletes it in the backward direction, $\cos\theta_{nL} < 0$, as shown in Fig. 5 for ^{235}U($n_{\rm th}$,f). The black curve shows the standard result, including the rotational boost, while the black circles show the effect of omitting that boost. No energy cut is applied to the emitted neutrons in either scenario. Also shown are the results for two scenarios where either only neutrons above 2 MeV or below 1 MeV are considered. (As expected from Fig. 4, the 2 MeV threshold enhances the relative yield in the forward direction, whereas the 1 MeV upper bound reduces the anisotropy.) In all three scenarios, there is little visible

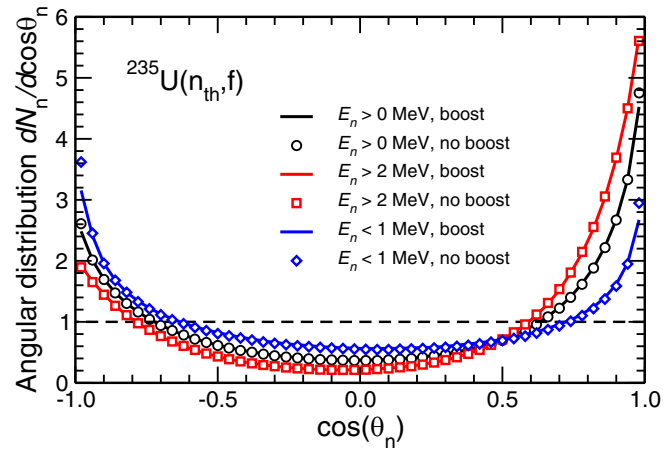

FIG. 5. The laboratory angular distribution of the evaporated neutrons from ^{235}U($n_{\rm th}$,f) relative to the direction of the light primary fragment, $dN_n/d\cos\theta_n$, is shown for both the standard FREYA scenario when the neutrons acquire a rotational boost (curves) and a modified scenario when this boost is omitted (symbols). In addition to considering neutrons of all energies (black), the figure also shows the result of including either only neutrons with energies above 2 MeV or below 1 MeV.

effect of the rotation. The largest deviations (still barely noticeable) occur near 0° and 180° and for the lowest neutron energies, which are the hardest to measure. Thus, even though there is a clear effect of the fragment rotation on the inherent neutron emission pattern, as expressed in Eqs. (8) and (9), it has a minimal influence on the observable angular distribution $dN_n/d\cos\theta_{nL}$. It thus seems unlikely that the fragment rotation can be determined experimentally on the basis of the one-neutron distribution alone.

B. Gated angular correlations

We now investigate the sensitivity of the neutron-neutron angular correlations to the angular momenta of the fragments. Because there is a close correlation between the fragment angular momentum and the total photon multiplicity, as shown in Fig. 3, this type of measurement could provide additional information on event-averaged neutron-photon correlations beyond those measured in Refs. [18–20], which do not provide a very clear picture. All three previous measurements are based on mass-averaged neutron and photon multiplicities in different TKE bins. Nifenecker *et al.* [18] suggested a strong positive correlation, Glassel *et al.* [19] saw a much weaker correlation, and Wang *et al.* [20] determined a more complex correlation by studying the correlation in different mass regions. Here we propose measuring the two-neutron angular correlations gating on the total photon multiplicity.

The general form of the correlation function has been discussed previously [21]. It can be readily understood from the dumbbell shape of the neutron velocity distribution shown in Fig. 4 that the distribution of the opening angle ϕ_{nn} is enhanced near 0° and 180°. For a more detailed understanding, we note that in the case considered, ^{235}U($n_{\rm th}$,f), the most probable outcome (22%) is that each fragment emits one neutron, which contributes near 180°. It is nearly as likely that the light fragment emits two neutrons and the heavy fragment one, giving two contributions near 180° and one near 0° (17% for each). Finally, it is somewhat less likely for the heavy fragment to emit two neutrons while the light fragment emits one, again yielding two contributions near 180° and one near 0° (10% for each). The greater number of contributions to the large-angle contribution, near 180°, results in a somewhat higher peak than at small angles, near 0°.

Figure 6(a) shows how the distribution of the opening angle between two detected neutrons, $P(\phi_{nn})$, depends on the energy of the neutrons and the combined spin magnitudes of the two primary fission fragments, averaged over all mass and charge partitions as well as the TKE distribution. Based on the combined spin magnitude, $S = S_L + S_H$, the fission events generated by FREYA are divided into either "low-spin" events ($S \leqslant 7\hbar$) or "high-spin" events ($S \geqslant 8\hbar$). A neutron angular correlation function is extracted separately for either "soft" ($E_n < 2$ MeV) or "hard" ($E_n > 2$ MeV) neutrons. It is evident that there is very little sensitivity to S, whereas the small-angle behavior of the correlation function depends significantly on the neutron energy. As expected from the velocity distribution in Fig. 4, the hard, energetic neutrons exhibit the expected enhancements near 0° and 180°, whereas the soft neutrons do not display a small-angle peak.

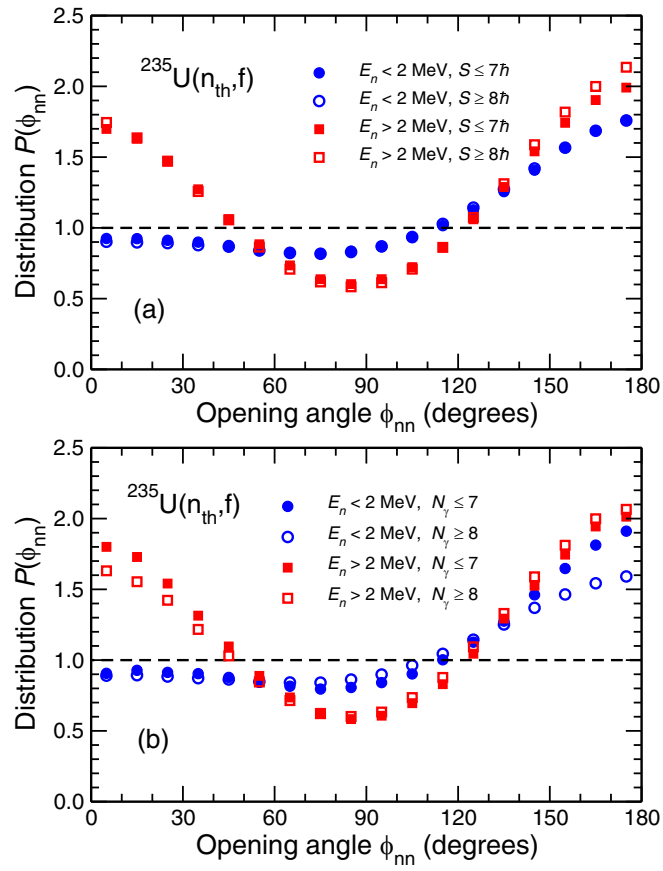

FIG. 6. Two-neutron angular correlations for ^{235}U($n_{\rm th}$,f), gating on either the total spin magnitude $S = S_L + S_H$ (a) or the total photon multiplicity N_γ (b). The angular correlation functions $P(\phi_{nn})$ for either "soft" neutrons ($E_n < 2$ MeV) or "hard" neutrons ($E_n > 2$ MeV) are presented in (a) for events with either a low or a high spin magnitude ($S \leqslant 7\hbar$ or $S \geqslant 8\hbar$, respectively) and in (b) for events with either a low or a high total photon multiplicity ($N_\gamma \leqslant 7$ or $N_\gamma \geqslant 8$, respectively).

As already discussed, although the spin magnitude S is not directly observable, the photon multiplicity may, to some degree, provide a proxy. To illustrate this possibility, Fig. 6(b) shows how the results in Fig. 6(a) are modified when the combined spin magnitude S is replaced by the total photon multiplicity N_γ. Here "photon-poor" events, having $N_\gamma \leqslant 7$, replace low-spin events and "photon-rich" events, with $N_\gamma \geqslant 8$, replace high-spin events. There is a greater sensitivity to N_γ than to S. There is a somewhat stronger small-angle enhancement for the photon-poor correlations with $E_n > 2$ MeV, while the large-angle peak is enhanced for low-energy neutrons in photon-poor events.

C. Projected angular correlations

A recent experimental investigation [6] introduced a new analysis method for extracting a dynamical anisotropy, the bulging of the neutron emission pattern caused by the rotation of the evaporating fragment. We employ FREYA to examine this idea in this section, enabling us to assess the importance

of the various effects that complicate the analysis. Because Ref. [6] studied ^{252}Cf(sf), we focus on this case here. However, we note that our findings apply generally.

The analysis [6] is based on the assumption that the fragment spins are perpendicular to the fragment motion. As we have discussed, in any given event, the angular distribution of the evaporated neutrons is (slightly) expanded in the plane transverse to the spin of the emitting nucleus (see Fig. 2). This plane is randomly oriented in a direction approximately perpendicular to the fragment velocity. If this is indeed so, then, in each event, the transverse distribution of the neutrons, obtained by projecting the full three-dimensional neutron velocity distribution onto the plane transverse to the motion of the light product nucleus, is also distorted. [If the contours of the full distribution are oblate spheroids with the symmetry axis along the fragment spin (hence perpendicular to the fragment velocity), then the contours of the projected distribution are ellipses with minor axes in that spin direction.] Consequently, the distribution of the neutron-neutron opening angles, ϕ_{nnL}, in the transverse plane is not entirely random but would exhibit slight enhancements around 0° and 180° [6].

The angular momenta of the primary fission fragments are determined at scission, at which point they are assumed to be perpendicular to the fission axis, the line between the centers of the two fledgling fragments, as described in Sec. II B. Subsequently, as the two fragments are being pushed apart by their mutual Coulomb repulsion, the line connecting their centers rotates somewhat due to the orbital motion of the dinuclear system. Furthermore, each evaporation process changes the magnitude and direction of both the linear and the angular momentum of the emitting nucleus. These effects complicate the extraction of the proposed correlation signal, as we now discuss.

We first consider a simplified scenario in which the relative fragment motion is purely radial, so there is no directional change of the dinuclear axis during the Coulomb acceleration, and no recoils are imparted to the fragments by evaporation. Then, to leading order, the undulating ϕ_{nnL} distribution is of the form $P(\phi_{nnL}) \sim 1 + c_2 \cos 2\phi_{nnL}$ with $c_2 > 0$. Because the amplitude c_2 increases approximately as the three-halves power of the anisotropy A, it is rather challenging to extract c_2 for small anisotropies. Therefore, to artificially enhance the signal for our present studies, we have increased the FREYA "spin temperature" parameter c_S from its standard value of 0.87 to 1.4. The mean light- and heavy-fragment spins are then $7.3\hbar$ and $9.0\hbar$ and the angular distribution of the evaporated neutrons relative to the spin direction of their respective mother fragments is characterized by an overall dynamical anisotropy of $A \approx 0.12$, a value rather similar to that obtained by Gavron [3].

If the neutrons are sampled from a common distribution with that anisotropy, the amplitude of the angular undulation of the projected opening angle would amount to $c_2 \approx 0.18\%$. However, there are two distinct anisotropic distributions in each fission event, one for each of the two fragments. Because the fragment spins are not mutually aligned (see Fig. 1), the resulting signal is correspondingly reduced. If the angle between the two spins were totally random, which is very nearly the case in FREYA as discussed in Sec. II B, then c_2 would be reduced by a factor of two.

To understand the effect of the various complications mentioned above, we start from a simplified scenario in which the dinuclear motion remains purely radial, as would be the case if the dinuclear complex had no orbital motion and the linear and angular momentum recoils were absent. In that ideal scenario, the undulation amplitude is $c_2 \approx 0.042\%$ if all the neutrons are included in the analysis. In an actual experiment, there is an energy threshold below which neutrons cannot be measured. Therefore, to conform with the experimental analysis [6], we use $E_{\min} = 0.9$ MeV in the following. This exclusion of the softest neutrons reduces the statistics by about one third, while it enhances the signal somewhat, to $c_2 \approx 0.058\%$. Generally, the FREYA simulations suggest that the effect grows steadily stronger as a function of the threshold energy $E_{\min}$.

The rotation of the dinuclear axis during the separation is typically about 2°. The rotation affects the signal by just a few percent because it merely causes a corresponding slight reorientation of the oblate velocity distributions relative to the fragment motion.

By contrast, the effect of the spin recoils is substantial, presumably because the evaporations change the spin direction considerably. On average, the rotational axis of the fragment changes its direction by about 9° as the result of an evaporation, producing a corresponding tilt in the angular distribution of the subsequent neutron. The FREYA simulations suggest that this effect can reduce the signal by more than a factor of two.

Finally, we address the recoils of the linear fragment momenta, which can significantly affect the extracted ϕ_{nnL} distribution. On average, the momentum recoil from an evaporation changes the direction of the fragment motion by only about 0.2°, consistent with the fragment being about 100 times heavier than the neutron. Even though this directional change is very small, it nevertheless affects the distribution of the projected opening angles to such a degree that the undulation signal is overwhelmed.

The signal is swamped because the recoil-induced change in the direction of fragment motion causes the transverse plane to be correspondingly tilted. As a particular consequence, the projected distribution of the neutrons from the heavy fragment is not centered at the origin of the tilted transverse plane but is shifted off center in the direction of the transverse velocity of the light fragment. This geometric feature, which is not related to the dynamic anisotropy, enhances the relative occurrence of small opening angles. The resulting modulation of the distribution of the projected opening angles is, to a good approximation, proportional to $\cos \phi_{nnL}$.

Thus the effect of the evaporation recoils and the effect of the dynamical anisotropy are largely independent. They can thus be extracted by performing a Fourier analysis of the distribution function,

$$P(\phi_{nnL}) \sim 1 + c_1 \cos \phi_{nnL} + c_2 \cos 2\phi_{nnL}. \qquad (10)$$

This approach has the additional advantage that the Fourier coefficients can be extracted with a reasonable degree of confidence even in the presence of large statistical errors on the individual values of $P(\phi_{nnL})$. This is an important advantage because quite large event samples are required for the extrac-

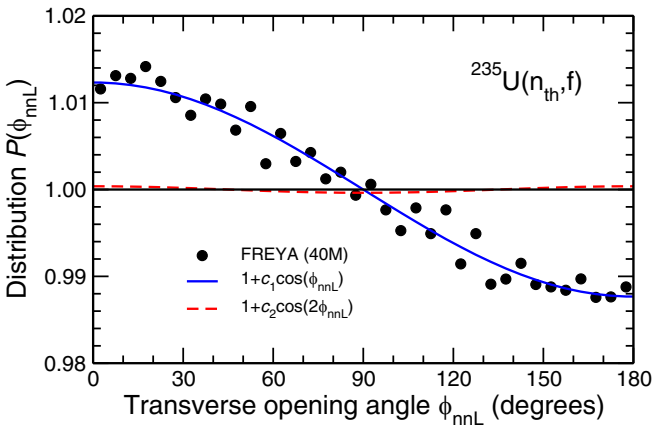

FIG. 7. The distribution of the neutron-neutron opening angle in the plane transverse to the direction of the light product nucleus, ϕ_{nnL}, is shown for ^{235}U($n_{\rm th}$,f) as obtained from 40 million FREYA events (filled circles). The extracted first and second Fourier components are also shown.

tion of this effect (tens of millions of events are needed in the FREYA simulations).

We finally note that the effects of the evaporation recoils and the rotational boosts are modified if separate analyses are made of neutron pairs that are emitted into opposite hemispheres (one is moving forward and the other backward, as seen in the laboratory) and neutron pairs emitted into the same hemisphere (both are either moving forward or backward). The FREYA simulations provide a quantitative impression of these effects. In the present scenario, with $c_S = 1.4$ rather than 0.87, FREYA yields $c_2 \approx 0.040\%$. If only pairs originating from the same hemisphere are included, then c_2 is reduced to about 0.020%, while it is increased to about 0.164% when only pairs from opposite hemispheres are included. For the same cases, c_1 is 1.3%, 1.2%, and 1.6%, respectively.

The results in the discussion so far are specific to ^{252}Cf obtained with FREYA for that case, but our discussion applies to other cases as well. Figure 7 shows the results for the case of primary interest in the present study, ^{235}U($n_{\rm th}$,f). We note that even though 40 million events were generated, the extracted distribution exhibits a considerable degree of statistical fluctuation. Nevertheless, it is possible to extract the Fourier coefficients c_1 and c_2 with reasonable confidence and the corresponding functions $1 + c_1 \cos\phi_{nnL}$ and $1 + c_2 \cos\phi_{nnL}$ are also shown. The first one, resulting from the evaporation recoils, dominates, while the undulations of the second one, reflecting the dynamical anisotropy, is more than an order of magnitude smaller and hardly visible.

IV. FISSION FROM ISOMERIC STATES

In neutron-induced fission, the target nucleus is usually in its ground state prior to the arrival of the neutron. However, in certain environments, both in nature and in the laboratory, there is a finite probability that the neutron absorption happens on an excited state of the target nucleus. This possibility is particularly likely when the target nucleus has a low-lying isomeric state. A prime example is ^{235}U, which we focus on here, whose first excited state lies at $E^* = 77$ eV and has a half-life of around 25 min [22,23]. This isomeric state, ^{235m}U, may readily be populated in the astrophysical environments occurring during the r process [24] or in terrestrial laser-generated plasmas [25]. The ^{235m}U($n_{\rm th}$,f) cross section was measured to be larger than the fission cross section of the ground state [26].

Here we seek to identify possible observable consequences of the target nucleus being in its isomeric state rather than its ground state when the incoming neutron arrives. To do this, we carry out FREYA simulations for two scenarios. The standard scenario corresponds to the case where the target nucleus ^{235}U is in its ground state. Because it has spin-$\frac{7}{2}$ the resulting compound nucleus can have angular momentum $S_0 = 3\hbar, 4\hbar$. We consider $S_0 = 4\,\hbar$. In the alternative scenario, the target nucleus ^{235}U is in its isomeric state at 77 eV. Because it has spin-$\frac{1}{2}$, the resulting compound nucleus can have $S_0 = 0,\ 1\hbar$. We consider $S_0 = 0$.

The potential-energy landscape for ^{236}U shows a well-developed mass-asymmetric valley beyond the second saddle (which is asymmetric). In addition, there is a pronounced mass-symmetric valley separated from the asymmetric valley by a down-sloping ridge. (The topography of the fission barrier landscape is brought out very well in Fig. 8 in Ref. [27].) At low energy, such as occurring in ^{235}U($n_{\rm th}$,f), the nuclear shape evolution takes the system over the lowest barrier and, consequently, down the asymmetric valley. The resulting fragment mass distribution is therefore asymmetric and the yield at symmetry is negligible. But as the energy is increased, it becomes ever easier for the shape to surmount the ridge and enter the symmetric valley. As a consequence, the mass distribution exhibits an ever more prominent symmetric component.

A recent study using microscopic many-body level densities to guide the Brownian shape evolution [28] found that the "leakage" into the symmetric valley is sensitive to the structure of the involved highly deformed nuclear shapes, in particular, to their pairing correlations, which may generally be larger than the shell effects in the barrier region. As a consequence, the symmetric yield has a delicate energy dependence (which may even be nonmonotonic). Furthermore, because the employed combinatorial method [29] provides the level density for different values of the total angular momentum S_0, it was possible also to study the dependence of the symmetric yield on S_0 [28]. It was found that the fragment mass distribution is generally rather insensitive to S_0 for moderate values up to $10\hbar$. However, the symmetric yield is significantly enhanced for $S_0 = 0$ due to pairing effects.

This finding is of particular interest in our present study, because the isomeric state in ^{235}U leads to compound spins of $S_0 = 0, 1\hbar$ with about equal probability, whereas the ground state leads to $S_0 = 3\hbar, 4\hbar$. In the latter case, for which extensive experimental data exist, the symmetric yield is very small, while the results reported in Ref. [28] suggest that for $S_0 = 0$ the symmetric mass yield is about 5% of the peak yield. We wish to explore the consequences of such a possible enhancement.

We have therefore constructed a mass distribution with a suitably enhanced symmetric yield to use as FREYA input. This is relatively easily done, because the usual input mass distri-

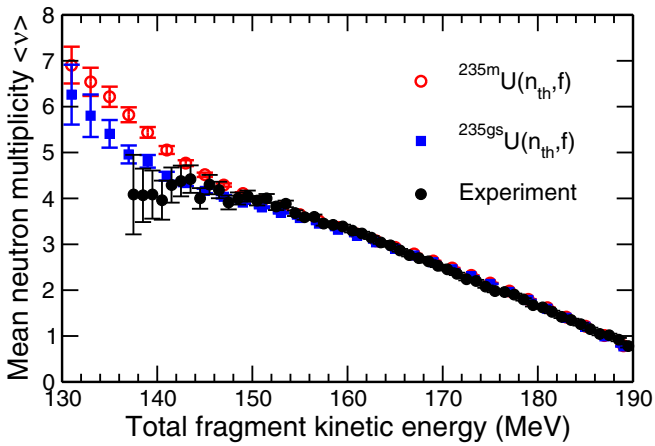

FIG. 8. The neutron multiplicity ν as a function of the TKE for ^{235}U($n_{\rm th}$,f) in two target scenarios: In the first scenario (filled blue squares), the target is the ground-state ^{235gs}U and the spin of the fissioning compound nucleus ^{236}U is $S_0 = 4\hbar$. In the alternative scenario (open red circles), the target is the isomeric-state ^{235m}U and $S_0 = 0$. In both cases, the symbols indicate the average multiplicities at the particular TKE. The dispersion of the multiplicity distribution at a given TKE is indicated by the error bars (so these are *not* uncertainties on the calculated results, which are based on 4×10^6 FREYA events). The experimental data (filled circles) are from Göök *et al.* [30].

bution is represented as the sum of a dominant asymmetric contribution and a small symmetric component [31]. We have increased the relative weight of the symmetric term to ensure $Y(\text{symm})/Y(\text{peak}) = 0.05$ and we use this modified mass distribution when simulating the alternative scenario where the target nucleus is in its isomeric state. We have left all other FREYA inputs unchanged, including the input TKE distribution TKE(A_H).

It is interesting to note that the two fission modes, asymmetric and symmetric, have other distinct characteristic features apart from the difference in their mass splits. In particular, the scission shapes of the symmetric mode tend to be significantly more elongated than those of the asymmetric mode [28,32]. Thus, in the symmetric mode the centers of the protofragments are typically farther apart than in the asymmetric mode and the potential energy at scission is correspondingly lower. This results in higher excitation energies at scission and lower fragment kinetic energies. Furthermore, the additional fragment excitation gained from the shape relaxation of the distorted protofragments [32] is also larger than in the asymmetric mode.

Of particular importance is the fact that the fission Q values tend to be larger than average for the symmetric mode (by ≈ 5.9 MeV). Therefore, when the symmetric component is enhanced, the overall average Q value will increase (by ≈ 290 keV); the concomitant change in the average neutron separation energy is much smaller (≈ 20 keV). Consequently, the average neutron multiplicity will increase (by ≈ 0.41), and because this increase arises from the symmetric component, it will appear at low TKE values.

TABLE I. Factorial moments of the neutron multiplicity distribution, $\mathcal{M}_n = \langle \nu(\nu-1)\ldots(\nu-n+1)\rangle$, for thermal fission using the ground state or the isomeric state of ^{235}U.

Case	$\mathcal{M}_1$	$\mathcal{M}_2$	$\mathcal{M}_3$	$\mathcal{M}_4$
^{235gs}U($n_{\rm th}$,f), $S_0 = 4\hbar$	2.39526	4.53167	6.46183	6.59926
^{235m}U($n_{\rm th}$,f), $S_0 = 0$	2.43591	4.75387	7.23551	8.62523

This is illustrated in Fig. 8, which shows the multiplicity of evaporated neutrons as a function of the TKE. The results for the two cases are effectively identical for TKE $\geqslant 150$ MeV but begin to separate for lower values where the higher probability of fission from the symmetric mode in the isomeric state tends to yield higher neutron multiplicities at low TKE. The data from Ref. [30], also shown in Fig. 8, are consistent with both calculations above 150 MeV but tend to agree more with the ground-state calculation, within the increasing statistical uncertainties, until TKE ≈ 140 MeV, where the data set ends. If data could be taken at still lower TKE, it might be possible to distinguish better between the two scenarios. Also, if isomeric-state targets could be fashioned and used to obtain a sufficiently significant data set, it might be feasible to measure a difference between the two scenarios. However, this would require a large number of isomeric targets to obtain enough low-TKE data to observe statistical differences.

On the theoretical side, these results were obtained only by an *ad hoc* modification of the mass yields, $Y(A)$, to enhance the yield at symmetry, consistent with the results in Ref. [28]. An improved calculation of the shape evolution for different values of S_0 would be required to obtain a more precise $Y(A)$ distribution to use in FREYA.

The enhanced neutron multiplicity at low TKE from an isomeric target should also manifest itself in an overall larger average neutron multiplicity and this is indeed the case. The neutron multiplicity distribution can be conveniently characterized by its factorial moments, $\mathcal{M}_n = \langle \nu(\nu-1)\ldots(\nu-$

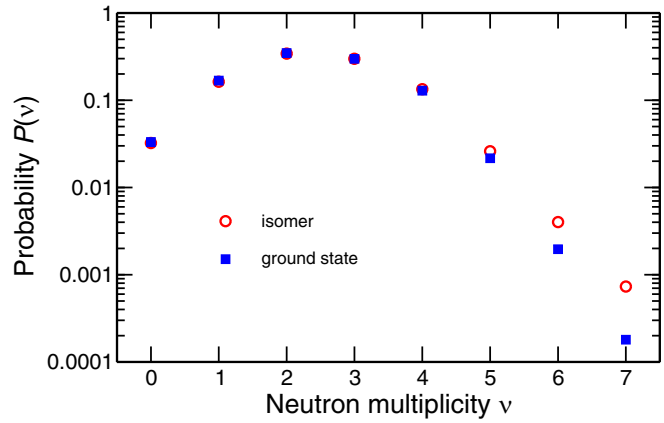

FIG. 9. The neutron multiplicity distribution $P(\nu)$ for the two cases of ^{235}U($n_{\rm th}$,f) shown in Fig. 8: ^{235gs}U (filled blue squares) and ^{235m}U (open red circles), shown on a logarithmic scale in order to better bring out the enhancement of high-multiplicity events.

$n+1)\rangle$. As reported in Table I, the average neutron multiplicity, the first factorial moment $\mathcal{M}_1$, is increased by 1.7%. As is evident in Fig. 8, the increase in the total multiplicity comes from the low-TKE events which yield the highest values of ν. The next three moments, $\mathcal{M}_2-\mathcal{M}_4$, are also listed in Table I. It is clear that fission from the isomeric state enhances the higher-multiplicity moments most. This can also be observed graphically in Fig. 9, presented on a logarithmic scale to more easily distinguish the high-multiplicity behavior.

V. CONCLUDING REMARKS

We have studied the role of angular momentum in the fission process to search for evidence of any quantitative effect it might have on fission observables. We employed FREYA in this study because it obeys all conservation laws throughout each step of a fission event, from scission through prompt neutron and photon evaporation. All of these analyses were carried out without changing FREYA inputs, unless otherwise noted. We have previously studied how changes in the spin temperature parameter, c_S, modifies the fragment rotational energy and thus affects photon observables; see Ref. [7] for details.

We have shown that, even if the initial compound nucleus is prepared with a definite angular momentum, which endows the fragments with correspondingly aligned average spins, the spin fluctuations acquired at scission ensure that there is little correlation between the resulting fragment spins and that of the compound nucleus. Furthermore, the spins of the two fragments are also essentially uncorrelated.

We showed that the total photon multiplicity is related to the combined magnitude of the two fragment spins, especially for $S_L + S_H > 5\hbar$ (see Fig. 3). We found that this effect is almost independent of the incident neutron energy, perhaps because, in FREYA, neutrons are emitted as long as energetically possible.

We have also studied neutron observables and found that neutron emission from a rotating fragment results in a oblate emission pattern, as first discussed in Ref. [12]. The resulting dynamical anisotropy increases with the fragment spin but it is hardly sensitive to the spin of the fissioning nucleus. Because the dynamical anisotropy is relatively small ($\sim$10%), it has hardly any observable influence on the neutron angular distribution with respect to the direction of the light fragment in the laboratory (see Fig. 5).

We have particularly focused on correlation observables. We discussed using neutron-neutron correlations gated on the photon multiplicity as a proxy for gating on the fragment angular momentum (see Fig. 6). While we found a weak dependence of the angular correlation on the photon multiplicity, we also showed that making a distinction between low- and high-energy neutrons has a stronger impact on the correlation function. Finally, we have discussed the projected neutron-neutron angular correlations proposed in Ref. [6] and found that even though the signal of the dynamical anisotropy is weak and is overwhelmed by the effect of evaporation recoils on the linear and angular momenta of the emitting fragments, it may be extracted by Fourier analysis (see Fig. 7).

In a separate analysis, we discussed possible observable effects of neutron-induced fission on the isomeric state of ^{235}U instead of a ^{235}U target in its ground state. For this, we employed a modified yield function $Y(A)$ to model the enhanced symmetric yield from a spin-0 ^{236}U compound nucleus obtained in Ref. [28] and found that this results in higher neutron multiplicities at low TKEs, a potentially observable effect that could distinguish fission from the isomer relative to the ground state (see Fig. 8). (It would obviously be very interesting to experimentally test the enhancement of the symmetric yield for spin-0 predicted in Ref. [28].)

In general, we have found that angular momentum effects are subtle and are generally insensitive to the spin of the initial state. While we have primarily focused on ^{235}U(n,f), we have found similar effects for other isotopes. The exception is fission from the low-lying uranium isomeric state where the predicted increase in the symmetric yield could have observable consequences if enough target material were available to accumulate sufficient statistics at low TKEs.

ACKNOWLEDGMENTS

This work was supported by the Office of Nuclear Physics, U.S. Department of Energy, under Contracts No. DE-AC02-05CH11231 (J.R.) and No. DE-AC52-07NA27344 (R.V.) and by the LLNL-LDRD Program under Project No. 20-ERD-031 (R.V.).

[1] J. B. Wilhelmy, E. Cheifetz, R. C. Jared, S. G. Thompson, H. R. Bowman, and J. O. Rasmussun, Angular momentum of primary products formed in the spontaneous fission of ^{252}Cf, Phys. Rev. C **5**, 2041 (1972).

[2] H. R. Bowman, S. G. Thompson, J. C. D. Milton, and W. J. Swiatecki, Velocity and angular distributions of prompt neutrons from spontaneous fission of ^{252}Cf, Phys. Rev. **126**, 2120 (1962).

[3] A. Gavron, Angular distributions of neutrons from fission fragments, Phys. Rev. C **13**, 2562 (1976).

[4] J. S. Pringle and F. D. Brooks, Angular Correlation of Neutrons from Spontaneous Fission of ^{252}Cf, Phys. Rev. Lett. **35**, 1563 (1975).

[5] A. S. Vorobyev *et al.*, Measurements of angular and energy distributions of prompt neutrons from thermal neutron-induced fission, Nucl. Instrum. Methods Phys. Res. Sec. A **598**, 795 (2009).

[6] A. Chietera *et al.*, Angular correlations in the prompt neutron emission of spontaneous fission of ^{252}Cf, Eur. Phys. J. A **54**, 98 (2018).

[7] R. Vogt and J. Randrup, Improved modeling of photon observables with the event-by-event fission model FREYA, Phys. Rev. C **96**, 064620 (2017).

[8] J. M. Verbeke, J. Randrup, and R. Vogt, Fission reaction event yield algorithm, FREYA—For event-by-event simulation of fission, Comput. Phys. Commun. **191**, 178 (2015).

[9] J. M. Verbeke, J. Randrup, and R. Vogt, Fission reaction event yield algorithm FREYA 2.0.2, Comput. Phys. Commun. **222**, 263 (2018).
[10] M. Bender *et al.*, Future of nuclear fission theory, J. Phys. G **47**, 113002 (2020).
[11] K.-H. Schmidt and B. Jurado, Review on the progress in nuclear fission—Experimental methods and theoretical descriptions, Prog. Prog. Phys. **81**, 106301 (2018).
[12] J. Randrup and R. Vogt, Refined treatment of angular momentum in FREYA, Phys. Rev. C **89**, 044601 (2014).
[13] T. Døssing and J. Randrup, Dynamical evolution of angular momentum in damped nuclear reactions: (I) Accumulation of angular momentum by nucleon transfer, Nucl. Phys. A **433**, 215 (1985).
[14] J. R. Nix and W. J. Swiatecki, Studies in the liquid-drop theory of nuclear fission, Nucl. Phys. **71**, 1 (1963).
[15] L. G. Moretto and R. P. Schmitt, Equilibrium statistical treatment of angular momenta associated with collective modes in fission and heavy-ion reactions, Phys. Rev. C **21**, 204 (1980).
[16] J. Randrup and R. Vogt, Calculation of fission observables through event-by-event simulation, Phys. Rev. C **80**, 024601 (2009).
[17] R. Capote *et al.*, RIPL–Reference Input Parameter Library for calculation of nuclear reactions and nuclear data evaluations, Nucl. Data Sheets **110**, 3107 (2009).
[18] H. Nifenecker, C. Signarbieux, M. Ribrag, J. Poitou, and J. Matuszek, Gamma-neutron competition in the de-excitation mechanism of the fission fragments, Nucl. Phys. A **189**, 285 (1972).
[19] P. Glâssel, R. Schmid-Fabian, D. Schwalm, D. Habs, and H. Helmolt, ^{252}Cf fission revisited: New insights into the fission process, Nucl. Phys. A **502**, 315 (1989).
[20] T. Wang *et al.*, Correlations of neutron multiplicity and γ-ray multiplicity with fragment mass and total kinetic energy in spontaneous fission of ^{252}Cf, Phys. Rev. C **93**, 014606 (2016).
[21] R. Vogt and J. Randrup, Neutron angular correlations in spontaneous and neutron-induced fission, Phys. Rev. C **90**, 064623 (2014).
[22] V. Zhudov, A. Zelenkov, V. Kulakov, M. Mostovoi, and B. Odinov, Differential spectrum of the conversion electrons and the excitation energy of (1/2+)-uranium-235 isomer, Pis'ma Zh. Eksp. Teor. Fiz. **30**, 549 (1979) [JETP Lett. **30**, 516 (1979)].
[23] M. R. Schmorak, Nuclear data sheets for $A = 231$, 235, 239, Nucl. Data Sheets **40**, 1 (1983).
[24] See, e.g., J. J. Cowan, C. Sneden, J. E. Lawler, A. Aprahamian, M. Wiescher, K. Langanke, G. Martinez-Pinedo, and F.-K. Thielemann, Origin of the heaviest elements: The rapid neutron-capture process, arXiv:1901.01410 [astro-ph.HE], and references therein.
[25] Y. Izawa and C. Yamanaka, Production of ^{235}U^{m} by nuclear excitation by electron transition in a laser produced uranium plasma, Phys. Lett. B **88**, 59 (1979).
[26] A. D'Eer, C. Wagemans, M. Néve de Mévergnies, F. Gönnenwein, P. Geltenbort, M. S. Moore, and J. Pauwels, Neutron-induced fission of the 26 min ^{235}U isomer, Phys. Rev. C **38**, 1270 (1988).
[27] T. Ichikawa, A. Iwamoto, P. Möller, and A. J. Sierk, Contrasting fission potential-energy structure of actinides and mercury isotopes, Phys. Rev. C **86**, 024610 (2012).
[28] D. E. Ward, B. G. Carlsson, T. Døssing, P. Möller, J. Randrup, and S. Åberg, Nuclear shape evolution based on microscopic level densities, Phys. Rev. C **95**, 024618 (2017).
[29] H. Uhrenholt, S. Åberg, A. Dobrowolski, T. Døssing, T. Ichikawa, and P. Möller, Combinatorial nuclear level-density model, Nucl. Phys. A **913**, 127 (2013).
[30] A. Göök, F.-J. Hambsch, S. Oberstedt, and M. Vidali, Prompt neutrons in correlation with fission fragments from ^{235}U(n, f), Phys. Rev. C **98**, 044615 (2018).
[31] U. Brosa, S. Grossmann, and A. Müller, Nuclear scission, Phys. Rep. **197**, 167 (1990).
[32] M. Albertsson, B. G. Carlsson, T. Døssing, P. Möller, J. Randrup, and S. Åberg, Correlation studies of fission fragment neutron multiplicities, arXiv:2005.09988 [nucl-th] [Phys. Rev. C (to be published)].